PAPER

Wall Admittance of a Circular Microstrip Antenna

Takafumi FUJIMOTO[†], **Kazumasa TANAKA**[†], *and* **Mitsuo TAGUCHI**[†], *Members*

SUMMARY The formulation of the wall admittance of a circular microstrip antenna by the spectral domain method is presented. The circular microstrip antenna is calculated using the cavity model. The electromagnetic fields within the antenna cavity are determined from the impedance boundary condition at the side aperture. The contribution from the region outside the antenna is taken into account by the wall admittance. The wall admittance is defined by the magnetic field produced by the equivalent magnetic current at the aperture. The magnetic field is calculated by the spectral domain method. The wall admittances obtained by this method are compared with the results calculated by Shen. The calculated input impedances of the microstrip antenna agree fairly well with the experimental data for the substrate thickness of up to $0.048\lambda_g$. The formulation of wall admittance presented here is easily applicable to arbitrarily shaped microstrip antennas.
key words: *microstrip antenna, wall admittance, spectral domain, cavity model, surface wave*

1. Introduction

The cavity model is a simple and efficient analytical method on microstrip antenna (MSA) of any configuration, where the separation of variables is possible in the wave equation expressed in the particular coordinate system [1]. In this method, the antenna is treated as a resonant cavity bounded above and below by the conducting plates and on the side by the admittance wall. The electromagnetic fields within the cavity are expanded in terms of the eigenfunctions. Therefore, the cavity model is conceptually simple and easily understandable compared with the solution obtained by the method of moments. The electromagnetic fields within the cavity are determined by the impedance boundary condition at the side aperture. The contribution from the region outside the antenna is taken into account by the wall admittance at the aperture. The accuracy of wall admittance affects the resonant frequency and the input impedance of the antenna.

The formulation of wall admittance of the MSA can be carried out by one of two methods. The first method is highly simple. The wall conductance of the rectangular MSA was obtained from the radiated power at the edge of the antenna and the susceptance from the capacitance of an open microstrip circuit [2], [3]. Shen [4] and Yano et al. [5] determined the wall admittance of a circular MSA from the radiated power and the fringe field at the edge of the antenna. The other method is based on the wall admittance defined by the magnetic field due to the equivalent magnetic current at the aperture. There are two methods to determine the magnetic fields in the external region. In the first method, Green's function in free space is used. A rectangular MSA and an annular ring MSA were analyzed by this method [6], [7]. The second method is more general and takes into account the effect of the dielectric substrate by spectral domain analysis. The circular and annular ring MSA were analyzed using the Hankel transform [8]. However, the wall admittance of arbitrarily shaped MSA cannot be calculated by these methods.

In this paper, a method for formulation of the wall admittance of an arbitrarily shaped MSA is proposed. As an example of arbitrarily shaped MSA, the circular MSA is calculated. The wall admittance is derived by spectral domain analysis to accurately estimate the effect of the dielectric substrate in the external region of the cavity. The magnetic field is expressed by Green's functions for the vector potential and the scalar potential due to the horizontally directed magnetic dipole. In order to apply Green's functions to arbitrarily shaped MSA, they are represented using the local coordinate system with the origin located at the antenna aperture. Green's functions are determined by applying the boundary conditions at the interfaces between free space, the dielectric substrate and ground plane to the solution of the wave equation in the spectral domain. Green's functions in the spatial domain are obtained by applying the inverse Fourier transform. Since the inverse Fourier transform is expressed by the infinite integral and contains poles associated with surface waves, the infinite integral is recast into the sum of closed form expression and finite integral [9], [10].

In order to ascertain the validity of the wall admittance obtained by the spectral domain method, the calculated input impedances of circular MSA are compared with the experimental data.

2. Electromagnetic Fields within the Cavity

Figure 1 shows a circular MSA and its coordinate system. The antenna is excited at $r = d_0$, $\phi = 0$ by

Manuscript received June 7, 1998.
Manuscript revised October 27, 1998.
[†]The authors are with the Department of Electrical and Electronic Engineering, Faculty of Engineering, Nagasaki University, Nagasaki-shi, 852-8521 Japan.

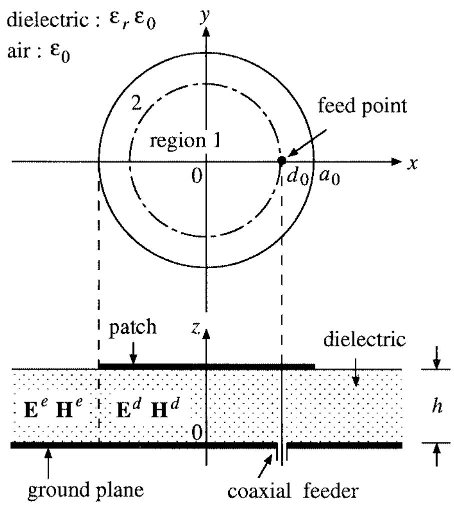

Fig. 1 Geometry of circular microstrip antenna.

a coaxial feeder through the dielectric substrate. The relative dielectric constant of the substrate is ε_r. The electromagnetic fields within and outside the cavity are denoted by $\mathbf{E}^d$, $\mathbf{H}^d$ and $\mathbf{E}^e$, $\mathbf{H}^e$, respectively.

The thickness of the substrate is assumed to be much smaller than the wavelength, so the electromagnetic fields within the cavity do not vary along the z direction. The z component of the electric field E_z^d satisfies the following Helmholtz equation in the cylindrical coordinate system (r, ϕ, z),

$$\left\{\frac{1}{r}\frac{\partial}{\partial r}(r\frac{\partial}{\partial r}) + \frac{1}{r^2}\frac{\partial^2}{\partial \phi^2} + {k_1}^2\right\} E_z^d(r,\phi) = 0 \tag{1}$$

where $k_1 = \omega\sqrt{\mu_0\varepsilon_1} = \omega\sqrt{\mu_0\varepsilon_r\varepsilon_0}$. In terms of Eq. (1) and Maxwell's equations, the electromagnetic fields within the cavity are expressed as,

$$\mathbf{E}^d = \sum_{n=0}^{N} \mathbf{i}_z E_{zn}^d(r,\phi) \tag{2}$$

$$\mathbf{H}^d = \sum_{n=0}^{N} \{\mathbf{i}_r H_{rn}^d(r,\phi) + \mathbf{i}_\phi H_{\phi n}^d(r,\phi)\} \tag{3}$$

In Region 1 $(0 \le r \le d_0)$

$$E_{zn}^d(r,\phi) = A_n J_n(k_1 r)\cos(n\phi) \tag{4}$$

$$H_{rn}^d(r,\phi) = -\frac{jn}{\omega\mu_0 r} A_n J_n(k_1 r)\sin(n\phi) \tag{5}$$

$$H_{\phi n}^d(r,\phi) = -\frac{jk_1}{\omega\mu_0} A_n J_n'(k_1 r)\cos(n\phi) \tag{6}$$

In Region 2 $(d_0 \le r \le a_0)$

$$E_{zn}^d(r,\phi) = \{B_n J_n(k_1 r) + C_n N_n(k_1 r)\}\cos(n\phi) \tag{7}$$

$$\begin{aligned} H_{rn}^d(r,\phi) \;=\; & -\frac{jn}{\omega\mu_0 r}\{B_n J_n(k_1 r) \\ & + C_n N_n(k_1 r)\}\sin(n\phi) \end{aligned} \tag{8}$$

$$\begin{aligned} H_{\phi n}^d(r,\phi) \;=\; & -\frac{jk_1}{\omega\mu_0}\{B_n J_n'(k_1 r) \\ & + C_n N_n'(k_1 r)\}\cos(n\phi) \end{aligned} \tag{9}$$

where $J_n(k_1 r)$ and $N_n(k_1 r)$ are Bessel and Neumann functions of order n, respectively. The prime denotes the derivative with respect to the argument. $\mathbf{i}_r$, $\mathbf{i}_\phi$ and $\mathbf{i}_z$ are unit vectors of the cylindrical coordinate system (r,ϕ,z). $\{A_n\}$, $\{B_n\}$ and $\{C_n\}$ are unknown coefficients to be determined from the boundary conditions between regions 1 and 2;

$$E_{z\,(region1)}^d = E_{z\,(region2)}^d,$$

$$H_{r\,(region1)}^d = H_{r\,(region2)}^d \,:\; r = d_0 \tag{10}$$

$$H_{\phi\,(region2)}^d - H_{\phi\,(region1)}^d = \frac{I_0}{d_0}\delta(\phi) \,:\; r = d_0 \tag{11}$$

and the impedance boundary condition at the aperture;

$$H_{\phi n}^d = -y_{sn} E_{zn}^d : \quad r = a_0, \tag{12}$$

where I_0 is the total current at the feed point and y_{sn} is the wall admittance of order n.

The equivalent magnetic current $\mathbf{M}$ at the aperture is given by

$$\mathbf{M} = \mathbf{E}^d \times \mathbf{n} \tag{13}$$

where $\mathbf{n}$ is the unit normal vector directed outward from the aperture. Substituting Eq. (7) into Eq. (13), the magnetic current is reduced to

$$\mathbf{M} = \mathbf{i}_\phi M = \sum_{n=0}^{N} \mathbf{i}_\phi M_n(\phi) \tag{14}$$

$$M_n(\phi) \;=\; \{B_n J_n(k_1 a_0) + C_n N_n(k_1 a_0)\}\cos(n\phi). \tag{15}$$

From the continuity condition on the tangential component of the magnetic field at the aperture, the wall admittance y_{sn} is defined by the magnetic field $H_{\phi n}^e$ produced by the equivalent magnetic current M_n at the aperture,

$$y_{sn} = -\frac{H_{\phi n}^e}{M_n}. \tag{16}$$

3. Magnetic Fields Outside the Cavity

In the formulation of the wall admittance, the local coordinate system (X, Y, Z) with the origin located at the point $(a_0, \phi', 0)$ in the cylindrical coordinate system is applied for arbitrarily shaped MSA. Figure 2 shows the local coordinate system. The positive X direction is defined by the tangential ϕ' direction. The

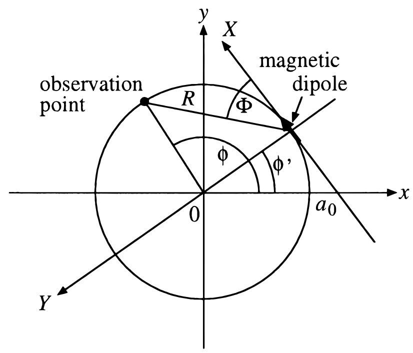

Fig. 2 Local coordinate system with origin located at antenna aperture.

observation point is located on the ground plane of the aperture $(a_0, \phi, 0)$ and the equivalent magnetic current exists at the aperture ($r{=}a_0$, $0 \le \phi' \le 2\pi$, $0 \le z' \le h$). Since the thickness of the substrate is assumed to be much smaller than the wavelength, the patch may be neglected in the externally equivalent problem. $\mathbf{H}^e$ is expressed by using the vector potential $\mathbf{F}$ and the scalar potential ϕ_m;

$$\mathbf{H}^e = -j\omega\mathbf{F} - \nabla\phi_m. \tag{17}$$

In terms of the transverse potential, the vector potential $\mathbf{F}$ is written as follows [10],

$$\mathbf{F} = \int_{aperture} (\mathbf{i}_X G_F^{XX} + \mathbf{i}_Y G_F^{YX}) M dS' \tag{18}$$

where G_F^{XX} and G_F^{YX} are X and Y components of Green's function for the vector potential due to a X-directed magnetic dipole, respectively. The scalar potential ϕ_m is written as follows,

$$\phi_m = \frac{1}{j\omega}\int_{aperture} \mathbf{M}\cdot(\nabla' G_V) dS' \tag{19}$$

where G_V is Green's function for the scalar potential. ∇ and ∇' are the derivative operators at the observation and source points, respectively. By substituting Eqs. (18) and (19) into Eq. (17), the magnetic field H_ϕ^e on the ground plane of the aperture $(a_0, \phi, 0)$ is given by the following equation,

$$\begin{aligned} H_{\phi n}^e = & -j\omega a_0 \int_0^{2\pi}\int_0^h \{\cos(\phi-\phi')G_F^{XX} \\ & + \sin(\phi-\phi')G_F^{YX}\} M_n \, dZ' d\phi' \\ & + \frac{1}{j\omega a_0}\int_0^{2\pi}\int_0^h \frac{\partial G_V}{\partial\phi}\frac{\partial M_n}{\partial\phi'}\, dZ' d\phi'. \end{aligned} \tag{20}$$

The Z component of the electric and magnetic fields created by a X-directed magnetic dipole are denoted by G_E^{ZX} and G_H^{ZX}, respectively. Using the notation "$^-$" for quantity in the spectral domain, $\overline{G}_F^{XX}$, $\overline{G}_F^{YX}$ and $\overline{G}_V$ are expressed as [10],

$$\overline{G}_F^{XX} = \frac{\varepsilon_1}{{k_R}^2{U_1}^2}(\omega\mu_0 k_X \frac{\partial\overline{G}_H^{ZX}}{\partial Z} - jk_Y {U_1}^2\,\overline{G}_E^{ZX}) \tag{21}$$

$$\overline{G}_F^{YX} = \frac{\varepsilon_1}{{k_R}^2{U_1}^2}(\omega\mu_0 k_Y \frac{\partial\overline{G}_H^{ZX}}{\partial Z} + jk_X {U_1}^2\,\overline{G}_E^{ZX}) \tag{22}$$

$$\overline{G}_V = \frac{\omega}{k_X {U_1}^2}\frac{\partial\overline{G}_H^{ZX}}{\partial Z} \tag{23}$$

$${U_1}^2 = {k_R}^2 - {k_1}^2 \tag{24}$$

$$k_X = k_R\cos\Theta, \quad k_Y = k_R\sin\Theta. \tag{25}$$

$\overline{G}_E^{ZX}$ or $\overline{G}_H^{ZX}$ in free space and the dielectric region are denoted as $\overline{\psi}_0$ and $\overline{\psi}_1$. $\overline{\psi}_1$ satisfies the wave equation in the spectral domain,

$$\left(\frac{d^2}{dZ^2} - {U_1}^2\right)\overline{\psi}_1 = \text{contribution of sources.} \tag{26}$$

The boundary conditions at the interface between free space and the dielectric are expressed as,

$$\alpha_0\overline{\psi}_0 = \alpha_1\overline{\psi}_1 \quad \text{and} \quad \frac{\partial\overline{\psi}_0}{\partial Z} = \frac{\partial\overline{\psi}_1}{\partial Z}, \quad \text{at } Z = h \tag{27}$$

where

$$\alpha_i = \begin{cases} \varepsilon_i : & \overline{\psi}_i = \overline{G}_E^{ZX} \\ \mu_0 : & \overline{\psi}_i = \overline{G}_H^{ZX} \end{cases} \quad (i = 0, 1),$$

and at the interface between the dielectric and ground plane,

$$\overline{G}_H^{ZX} = 0 \quad \text{and} \quad \frac{\partial\overline{G}_E^{ZX}}{\partial Z} = 0, \quad \text{at } Z = 0. \tag{28}$$

By applying the boundary conditions (27) and (28) to the solutions of the wave equation (26), $\overline{G}_E^{ZX}$ and $\overline{G}_H^{ZX}$ are obtained. Green's functions in the spatial domain G_F^{XX}, G_F^{YX} and G_V are derived by applying the inverse Fourier transform to $\overline{G}_F^{XX}$, $\overline{G}_F^{YX}$ and $\overline{G}_V$ (see Appendix A). By substituting $Z = 0$ into Eqs. (A· 17)–(A· 19) in Appendix A, the spatial domain Green's functions on the ground plane of the aperture $(a_0, \phi, 0)$ are expressed by the following equations,

$$\begin{aligned} G_F^{XX} = & \frac{\varepsilon_1}{4\pi}\int_0^\infty \{g_{fX}^L(k_R) \\ & - g_{fY}^L(k_R)\cos(2\Phi)\} dk_R \end{aligned} \tag{29}$$

$$G_F^{YX} = -\frac{\varepsilon_1}{4\pi}\int_0^\infty g_{fY}^L(k_R)\sin(2\Phi) dk_R \tag{30}$$

$$\frac{\partial G_V}{\partial\phi} = \frac{-{a_0}^2\sin(\phi-\phi')}{2\pi\mu_0 R}\int_0^\infty g_V^L(k_R) dk_R \tag{31}$$

$$g_{fX}^L(k_R) = \left\{\frac{P_3(0)}{\varDelta_H} + \frac{P_4(0)}{\varDelta_E}\right\}\frac{k_R}{U_1}J_0(k_R R) \tag{32}$$

$$g^L_{fY}(k_R) = \left\{ \frac{P_3(0)}{\Delta_H} - \frac{P_4(0)}{\Delta_E} \right\} \frac{k_R}{U_1} J_2(k_R R) \tag{33}$$

$$g^L_V(k_R) = \frac{P_3(0)}{\Delta_H} \frac{{k_R}^2}{U_1} J_1(k_R R) \tag{34}$$

$$\begin{aligned} P_3(0) &= U_1 \sinh\{U_1(h - Z')\} \\ &\quad + U_0 \cosh\{U_1(h - Z')\} \end{aligned} \tag{35}$$

$$\begin{aligned} P_4(0) &= \varepsilon_1 U_0 \sinh\{U_1(h - Z')\} \\ &\quad + \varepsilon_0 U_1 \cosh\{U_1(h - Z')\} \end{aligned} \tag{36}$$

$$R = a_0 \sqrt{2 - 2\cos(\phi - \phi')} \tag{37}$$

$$\Phi = \left\{ \begin{array}{lll} \pi - \frac{1}{2}(\phi' - \phi) & : & \phi' \geq \phi \\ \frac{1}{2}(\phi - \phi') & : & \phi > \phi', \end{array} \right. \tag{38}$$

where Δ_E and Δ_H are expressed by Eqs. (A·11) and (A·12) in Appendix A, respectively. Substituting Eqs. (29)–(31) into Eq. (20), the magnetic field H^e_ϕ is obtained.

By subtracting the quasi-static terms from the integrands (32) and (34), the remaining integrands decay faster for larger k_R [9], [10]. The poles associated with the surface waves exist for Δ_E=0. The contributions from the poles are evaluated analytically by means of the residue calculus technique, and the wall conductance due to these poles is obtained by Eq. (A·36) (see Appendix B).

4. Input Impedance

By applying Poynting's theorem to the volume V enclosed by the surface S consisting of the patch, the ground plane and the aperture, the input impedance of MSA is defined as [4]

$$Z_{in} = \frac{\frac{1}{2} V_0 {V_0}^*}{P^* + P_d + P_c - 2j\omega(W_m - W_e)} \tag{39}$$

where

$$P = \frac{1}{2} \int_{aperture} (\mathbf{E}^e \times \mathbf{H}^{e*}) \cdot \mathbf{n} dS \tag{40}$$

$$W_e = \frac{1}{4} \int_V \varepsilon' |\mathbf{E}^d|^2 dV \tag{41}$$

$$W_m = \frac{1}{4} \int_V \mu_0 |\mathbf{H}^d|^2 dV \tag{42}$$

$$P_d = \frac{1}{2} \int_V \omega\varepsilon'' |\mathbf{E}^d|^2 dV \tag{43}$$

$$P_c = \frac{1}{2} \int_{conductor} \sigma |\mathbf{E}^d|^2 dS. \tag{44}$$

$\mathbf{n}$ is the unit normal vector on the surface S. σ is the conductivity of the patch and the ground plane and $\varepsilon_1 = \varepsilon_r \varepsilon_0 = \varepsilon' - j\varepsilon''$. The real part of P represents the radiated power leaving the aperture. The imaginary part of P represents the stored energy of the fringe field around the aperture. P_d and P_c are the power dissipated in V due to the dielectric and conductor losses, respectively. W_e and W_m are the electric and magnetic energies stored in V, respectively. V_0 is the voltage across the patch and the ground plane at the feed point $r = d_0, \phi = 0$.

By substituting Eqs. (2)–(9) into Eqs. (40)–(44), the following expressions are obtained.

$$\begin{aligned} P &= \frac{\pi a_0 h}{2} \sum_{n=0}^{N} (1 + \delta_n) {y_{sn}}^* \\ &\quad \times |B_n J_n(k_1 a_0) + C_n N_n(k_1 a_0)|^2 \end{aligned} \tag{45}$$

$$\begin{aligned} W_e &= \frac{\varepsilon' \pi h}{4} \sum_{n=0}^{N} (1 + \delta_n) [|A_n|^2 \int_0^{d_0} r {J_n}^2(k_1 r) dr \\ &\quad + \int_{d_0}^{a_0} r\{|B_n|^2 {J_n}^2(k_1 r) + |C_n|^2 {N_n}^2(k_1 r) \\ &\quad + (B_n {C_n}^* + {B_n}^* C_n) J_n(k_1 r) N_n(k_1 r)\} dr] \end{aligned} \tag{46}$$

$$\begin{aligned} W_m &= \frac{\pi h}{4\omega^2 \mu_0} \sum_{n=1}^{N} n^2 [|A_n|^2 \int_0^{d_0} \frac{{J_n}^2(k_1 r)}{r} dr \\ &\quad + \int_{d_0}^{a_0} \frac{1}{r} \{|B_n|^2 {J_n}^2(k_1 r) + |C_n|^2 {N_n}^2(k_1 r) \\ &\quad + (B_n {C_n}^* + {B_n}^* C_n) J_n(k_1 r) N_n(k_1 r)\} dr] \\ &\quad + \frac{\pi h {k_1}^2}{4\omega^2 \mu_0} \sum_{n=0}^{N} (1 + \delta_n) [|A_n|^2 \int_0^{d_0} r {J'_n}^2(k_1 r) dr \\ &\quad + \int_{d_0}^{a_0} r\{|B_n|^2 {J'_n}^2(k_1 r) + |C_n|^2 {N'_n}^2(k_1 r) \\ &\quad + (B_n {C_n}^* + {B_n}^* C_n) J'_n(k_1 r) N'_n(k_1 r)\} dr] \end{aligned} \tag{47}$$

$$P_d = 2\omega \tan\delta W_e \tag{48}$$

$$P_c = \frac{2\omega\delta_s}{h} W_m \tag{49}$$

In the above expressions δ_n is zero for $n > 0$ and is equal to 1 for $n = 0$, $\tan\delta = \varepsilon''/\varepsilon'$ is the loss tangent of the dielectric substrate and $\delta_s = (\pi\mu_0\sigma f)^{-\frac{1}{2}}$ is the skin depth of the conducting plate at the operating frequency f.

5. Results and Discussion

Figure 3 shows the wall conductances of the first mode g_{s1} calculated by the spectral domain method and g_{r1} by Shen's method [4]. The wall conductance due to the surface wave g^{sw}_{s1} included in g_{s1} is also shown in Fig. 3. In Shen's method, the wall conductance is determined from the radiated power at the edge of the

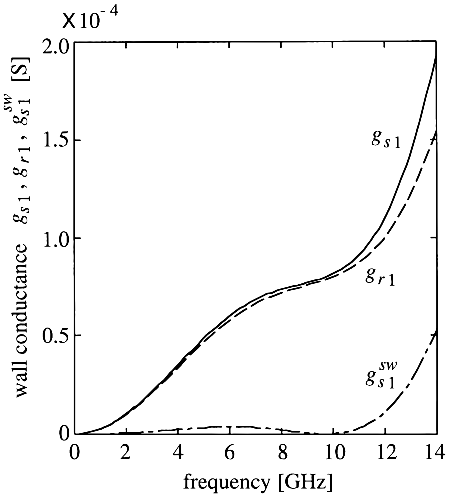

Fig. 3 Wall conductances of first mode ($a_0 = 9.0$ mm, $h = 0.764$ mm, $\varepsilon_r = 2.15$).

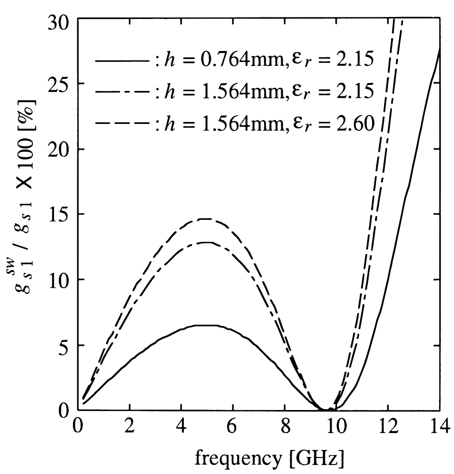

Fig. 4 Ratio of surface wave conductance to wall conductance (a_0=9.0 mm, first mode).

antenna. Around the resonant frequency of the first mode (6.4 GHz) and at higher frequencies, a difference between g_{s1} and g_{r1} is observed. This difference is due to the effect of the surface wave. g_{s1}^{sw} expressed by Eq. (A· 36) in Appendix B vanishes at around 9.5 GHz [8]. Since the wave number of the TM_{110} mode is not used in Eqs. (4)–(9), g_{s1}^{sw} includes the surface wave conductances of TM_{1m0} modes (m=2, 3, ...). Figure 4 shows the ratio of g_{s1}^{sw} to g_{s1} for different values of dielectric constant ε_r and thickness h. The rate of g_{s1}^{sw} increases as the dielectric constant and thickness increase. Therefore, the effect of the surface wave should be considered in the calculation of wall conductance for the thicker dielectric substrate.

Figure 5 shows the wall susceptances of the first mode b_{s1} calculated by the spectral domain method and b_{r1} by Shen's method. In Shen's method, the wall susceptance is determined from the fringe field at the edge of the antenna. Although b_{r1} is only valid at the

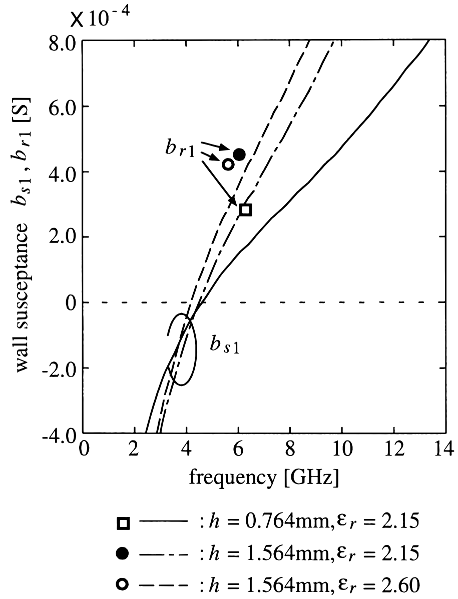

Fig. 5 Wall susceptances of first mode (a_0=9.0 mm).

resonant frequency [11], b_{s1} can be calculated at all frequencies.

Figures 6(a) and (b) show the calculated and measured input impedances of the circular MSA. In the numerical calculation, the number of modes N is determined to be 5 to obtain the convergent solution. Thicknesses of the dielectric substrate in Figs. 6(a) and (b) are $0.024\lambda_g$ and $0.048\lambda_g$, respectively. λ_g is the wavelength within the dielectric at the resonant frequency of the MSA. The antennas are made of copper-clad Glass-fiber-PTFE. Fairly good agreements between the calculated and the experimental results are observed. The relative errors of the measured resonant frequency to the calculated one are 1.1% at $0.024\lambda_g$ and 1.6% at $0.048\lambda_g$, respectively. The relative errors increase fractionally as the thickness of dielectric substrate increases. This error is due to the assumption that the equivalent magnetic current is uniform in the z direction.

6. Conclusion

The wall admittance of the circular MSA has been formulated by the spectral domain method. In this paper, the wall admittance is defined by the magnetic field due to the equivalent magnetic current at the aperture. In the spectral domain analysis, MSA is modeled as a layered medium consisting of free space, a dielectric with a magnetic dipole and a ground plane. The wall admittance calculated by the spectral domain method is compared with the one given by Shen, commonly used in the analysis of the circular MSA. The wall admittance formulated here includes the wall conductance due to the surface waves. The contribution of surface wave conductance to wall conductance is significant around

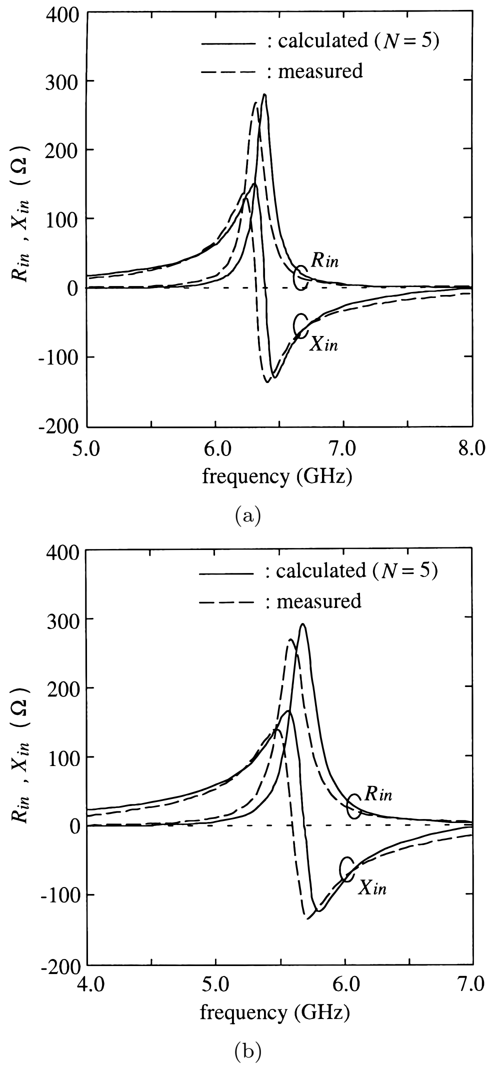

Fig. 6 Input impedances of circular microstrip antenna.
(a) a_0=9.05 mm, d_0=6.0 mm, h=0.764 mm, ε_r=2.15, $\tan\delta$=0.001
(b) a_0=9.06 mm, d_0=6.0 mm, h=1.564 mm, ε_r=2.60, $\tan\delta$=0.022.

the resonant frequency of first mode and at the higher frequencies. Although the wall susceptance by Shen's method is only valid at the resonant frequency, that by the spectral domain method can be obtained at all frequencies.

In order to ascertain the validity of the wall admittance calculated here, the input impedances of the probe-fed MSA have been calculated by the cavity model and compared with the experimental results. It is assumed in the cavity model that the thickness of the substrate is much smaller than the wavelength and the patch, ground plane and dielectric are lossless. The probe feed is replaced by the delta-function generator. Although the input impedance is expressed as the ratio of the voltage across the patch and the ground plane to the feed point current, the input impedance is formulated here by Poynting's theorem in order to consider the conductor loss and the dielectric loss. The calculated input impedances agree fairly well with the measured data for the substrate thickness from $0.024\lambda_g$ to $0.048\lambda_g$.

The wall admittance of arbitrarily shaped patch MSA is easily obtained by using the method presented here. MSA with thicker dielectric substrate could be calculated accurately by considering the variation of electromagnetic fields in the z direction.

Acknowledgement

The input impedances of MSA were measured at the Joint Research and Development Center, Saga University. The authors would like to thank Research Associate E. Nishiyama of Saga University for his valuable advice on the measurement of MSA.

References

[1] Y.T. Lo, D. Solomon, and W.F. Richards, "Theory and experiment on microstrip antennas," IEEE Trans. Antennas & Propag., vol.AP-27, no.2, pp.137–145, March 1979.
[2] A.G. Derneryd, "Linearly polarized microstrip antennas," IEEE Trans. Antennas & Propag., vol.AP-24, no.6, pp.846–851, Nov. 1976.
[3] K.R. Carver and J.W. Mink, "Microstrip antenna technology," IEEE Trans. Antennas & Propag., vol.AP-29, no.1, pp.2–24, Jan. 1981.
[4] L.C. Shen, "Analysis of circular-disc printed-circuit antenna," Proc. IEE, vol.126, no.12, pp.1220–1222, Dec. 1979.
[5] S. Yano and A. Ishimaru, "Theoretical study of the input impedance of circular microstrip disk antenna," IEEE Trans. Antennas & Propag., vol.AP-29, no.1, pp.77–83, Jan. 1981.
[6] A.K. Bhattacharyya and R. Garg, "Generalised transmission line model for microstrip patches," Proc. IEE, vol.132, Pt.H, no.2, pp.93–98, April 1985.
[7] A.K. Bhattacharyya and R. Garg, "Input impedance of annular ring microstrip antenna using circuit theory approach," IEEE Trans. Antennas & Propag., vol.AP-33, no.4, pp.369–374, April 1985.
[8] A.K. Bhattacharyya and R. Garg, "Spectral domain analysis of wall admittances for circular and annular microstrip patches and the effect of surface waves," IEEE Trans. Antennas & Propag., vol.AP-33, no.10, pp.1067–1073, Oct. 1985.
[9] M.I. Aksun and R. Mittra, "Derivation of closed-form Green's functions for a general microstrip geometry," IEEE Trans. Microwave Theory & Tech., vol.40, no.11, pp.2055–2062, Nov. 1992.
[10] J.R. Mosig, "Integral equation technique," ed. T. Itoh, in Numerical techniques for microwave and millimeter-wave passive structures, pp.133–213, John Wiley & Sons, New York, 1989.
[11] L.C. Shen, S.A. Long, M.R. Allerding, and M.D. Walton, "Resonant frequency of a circular disc, printed-circuit antenna," IEEE Trans. Antennas & Propag., vol.AP-25, pp.595–596, July 1977.

Appendix A: Spatial Domain Green's Functions for the Vector and Scalar Potential

Green's functions in the spectral domain $\overline{G}_F^{XX}$, $\overline{G}_F^{YX}$ and $\overline{G}_V$ are obtained by substituting $\overline{G}_E^{ZX}$ and $\overline{G}_H^{ZX}$ into Eqs. (21)–(23)[10].

$Z' \leq Z \leq h$

$$\overline{G}_F^{XX} = \frac{\varepsilon_1}{2\pi U_1}\{\frac{P_1(Z)}{\Delta_H}\cos^2\Theta + \frac{P_2(Z)}{\Delta_E}\sin^2\Theta\} \tag{A$\cdot$ 1}$$

$$\overline{G}_F^{YX} = \frac{\varepsilon_1}{2\pi U_1}\{\frac{P_1(Z)}{\Delta_H} - \frac{P_2(Z)}{\Delta_E}\}\cos\Theta\sin\Theta \tag{A$\cdot$ 2}$$

$$\overline{G}_V = \frac{P_1(Z)}{2\pi\mu_0 U_1 \Delta_H} \tag{A$\cdot$ 3}$$

$0 \leq Z \leq Z'$

$$\overline{G}_F^{XX} = \frac{\varepsilon_1}{2\pi U_1}\{\frac{P_3(Z)}{\Delta_H}\cos^2\Theta + \frac{P_4(Z)}{\Delta_E}\sin^2\Theta\} \tag{A$\cdot$ 4}$$

$$\overline{G}_F^{YX} = \frac{\varepsilon_1}{2\pi U_1}\{\frac{P_3(Z)}{\Delta_H} - \frac{P_4(Z)}{\Delta_E}\}\cos\Theta\sin\Theta \tag{A$\cdot$ 5}$$

$$\overline{G}_V = \frac{P_3(Z)}{2\pi\mu_0 U_1 \Delta_H} \tag{A$\cdot$ 6}$$

In the above equations

$$\begin{aligned} P_1(Z) = {} & [U_1 \sinh\{U_1(h-Z)\} \\ & + U_0 \cosh\{U_1(h-Z)\}]\cosh(U_1 Z') \end{aligned} \tag{A$\cdot$ 7}$$

$$\begin{aligned} P_2(Z) = {} & [\varepsilon_1 U_0 \sinh\{U_1(h-Z)\} \\ & + \varepsilon_0 U_1 \cosh\{U_1(h-Z)\}] \\ & \times \cosh(U_1 Z') \end{aligned} \tag{A$\cdot$ 8}$$

$$\begin{aligned} P_3(Z) = {} & [U_1 \sinh\{U_1(h-Z')\} \\ & + U_0 \cosh\{U_1(h-Z')\}]\cosh(U_1 Z) \end{aligned} \tag{A$\cdot$ 9}$$

$$\begin{aligned} P_4(Z) = {} & [\varepsilon_1 U_0 \sinh\{U_1(h-Z')\} \\ & + \varepsilon_0 U_1 \cosh\{U_1(h-Z')\}] \\ & \times \cosh(U_1 Z) \end{aligned} \tag{A$\cdot$ 10}$$

$$\Delta_E = \varepsilon_0 U_1 \sinh(U_1 h) + \varepsilon_1 U_0 \cosh(U_1 h) \tag{A$\cdot$ 11}$$

$$\Delta_H = U_1 \cosh(U_1 h) + U_0 \sinh(U_1 h). \tag{A$\cdot$ 12}$$

Green's functions in the spatial domain are obtained by applying the inverse Fourier transform to Eqs. (A$\cdot$ 1)–(A$\cdot$ 6). The inverse Fourier transform is defined as

$$\begin{aligned} g(X,Y,Z) = {} & \frac{1}{2\pi}\int_0^\infty k_R \int_0^{2\pi} \overline{g}(k_R,\Theta) \\ & \times \exp\{jk_R R\cos(\Theta-\Phi)\}d\Theta dk_R. \end{aligned} \tag{A$\cdot$ 13}$$

Consequently, Green's functions in the spatial domain at any point (X, Y, Z) are expressed by the following equations,

$Z' \leq Z \leq h$

$$\begin{aligned} G_F^{XX} = {} & \frac{\varepsilon_1}{4\pi}\int_0^\infty \{g_{fX}^U(k_R) \\ & - g_{fY}^U(k_R)\cos(2\Phi)\}dk_R \end{aligned} \tag{A$\cdot$ 14}$$

$$G_F^{YX} = -\frac{\varepsilon_1}{4\pi}\int_0^\infty g_{fY}^U(k_R)\sin(2\Phi)dk_R \tag{A$\cdot$ 15}$$

$$\frac{\partial G_V}{\partial \phi} = \frac{-{a_0}^2\sin(\phi-\phi')}{2\pi\mu_0 R}\int_0^\infty g_V^U(k_R)dk_R \tag{A$\cdot$ 16}$$

$0 \leq Z \leq Z'$

$$\begin{aligned} G_F^{XX} = {} & \frac{\varepsilon_1}{4\pi}\int_0^\infty \{g_{fX}^L(k_R) \\ & - g_{fY}^L(k_R)\cos(2\Phi)\}dk_R \end{aligned} \tag{A$\cdot$ 17}$$

$$G_F^{YX} = -\frac{\varepsilon_1}{4\pi}\int_0^\infty g_{fY}^L(k_R)\sin(2\Phi)dk_R \tag{A$\cdot$ 18}$$

$$\frac{\partial G_V}{\partial \phi} = \frac{-{a_0}^2\sin(\phi-\phi')}{2\pi\mu_0 R}\int_0^\infty g_V^L(k_R)dk_R \tag{A$\cdot$ 19}$$

where

$$g_{fX}^U(k_R) = \{\frac{P_1(Z)}{\Delta_H} + \frac{P_2(Z)}{\Delta_E}\}\frac{k_R}{U_1}J_0(k_R R) \tag{A$\cdot$ 20}$$

$$g_{fY}^U(k_R) = \{\frac{P_1(Z)}{\Delta_H} - \frac{P_2(Z)}{\Delta_E}\}\frac{k_R}{U_1}J_2(k_R R) \tag{A$\cdot$ 21}$$

$$g_V^U(k_R) = \frac{P_1(Z)}{\Delta_H}\frac{{k_R}^2}{U_1}J_1(k_R R) \tag{A$\cdot$ 22}$$

$$g_{fX}^L(k_R) = \{\frac{P_3(Z)}{\Delta_H} + \frac{P_4(Z)}{\Delta_E}\}\frac{k_R}{U_1}J_0(k_R R) \tag{A$\cdot$ 23}$$

$$g_{fY}^L(k_R) = \{\frac{P_3(Z)}{\Delta_H} - \frac{P_4(Z)}{\Delta_E}\}\frac{k_R}{U_1}J_2(k_R R) \tag{A$\cdot$ 24}$$

$$g_V^L(k_R) = \frac{P_3(Z)}{\Delta_H}\frac{{k_R}^2}{U_1}J_1(k_R R). \tag{A$\cdot$ 25}$$

Appendix B: Derivation of the Wall Conductance due to the Surface Wave [9],[10]

Figure A·1 shows the integration path of Eqs. (29) and (30). The integration interval is decomposed into three

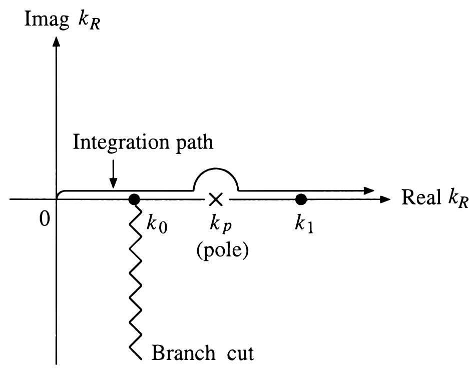

Fig. A·1 Integration path of inverse Fourier transform (29) and (30).

subintervals, $[0, k_0]$, $[k_0, k_1]$ and $[k_1, \infty]$. In the interval $[k_0, k_1]$, the pole associated with the surface wave exists for Δ_E=0. Therefore, the integrals of g^L_{fX} and g^L_{fY} along the interval $[k_0, k_1]$ are recast into the following expression.

$$\int_{k_0}^{k_1} g^L_{fX}(k_R)dk_R = \int_{k_0}^{k_1} \{g^L_{fX}(k_R) - F_X(k_R)\}dk_R + \int_{k_0}^{k_1} F_X(k_R)dk_R \quad \text{(A·26)}$$

$$\int_{k_0}^{k_1} g^L_{fY}(k_R)dk_R = \int_{k_0}^{k_1} \{g^L_{fY}(k_R) - F_Y(k_R)\}dk_R + \int_{k_0}^{k_1} F_Y(k_R)dk_R \quad \text{(A·27)}$$

where

$$F_X(k_R) = \frac{Res_X}{k_R - k_p} \quad \text{(A·28)}$$

$$Res_X = \lim_{k_R \to k_p} \frac{P_4(0)k_R J_0(k_R R)(k_R - k_p)}{U_1 \Delta_E} = \lim_{k_R \to k_p} \frac{P_4(0)k_R J_0(k_R R)}{\dfrac{d}{dk_R} U_1 \Delta_E} \quad \text{(A·29)}$$

$$F_Y(k_R) = \frac{Res_Y}{k_R - k_p} \quad \text{(A·30)}$$

$$Res_Y = \lim_{k_R \to k_p} \frac{-P_4(0)k_R J_2(k_R R)(k_R - k_p)}{U_1 \Delta_E} = \lim_{k_R \to k_p} \frac{-P_4(0)k_R J_2(k_R R)}{\dfrac{d}{dk_R} U_1 \Delta_E}, \quad \text{(A·31)}$$

and k_p is the surface wave pole located on the real axis of the complex k_R. The integrals of Res_X and Res_Y are the residues of $F_X(k_R)$ and $F_Y(k_R)$ at the pole k_p, respectively. The integrals of $F_X(k_R)$ and $F_Y(k_R)$ are analytically calculated as follows.

$$\int_{k_0}^{k_1} F_X(k_R)dk_R = Res_X(\ln \frac{k_1 - k_p}{k_p - k_0} - j\pi) \quad \text{(A·32)}$$

$$\int_{k_0}^{k_1} F_Y(k_R)dk_R = Res_Y(\ln \frac{k_1 - k_p}{k_p - k_0} - j\pi) \quad \text{(A·33)}$$

Substituting the second terms on the right-hand sides of Eqs. (A·32) and (A·33) into Eqs. (29) and (30), Green's functions due to the surface wave become

$$G_F^{XX} = -j\pi \frac{\varepsilon_1}{4\pi}\{Res_X - Res_Y \cos(2\Phi)\} \quad \text{(A·34)}$$

$$G_F^{YX} = -j\pi \frac{\varepsilon_1}{4\pi}\{-Res_Y \sin(2\Phi)\}. \quad \text{(A·35)}$$

Therefore, the wall conductance due to the surface wave g^{sw}_{sn} is summarized as

$$g^{sw}_{sn} = \frac{\omega a_0 \varepsilon_1}{4M_n} \int_0^{2\pi} \int_0^h [\cos(\phi - \phi')Res_X - \{\cos(2\Phi)\cos(\phi - \phi') + \sin(2\Phi)\sin(\phi - \phi')\}Res_Y] M_n dZ' d\phi'. \quad \text{(A·36)}$$

Takafumi Fujimoto received his B.E and M.E. degrees from Nagasaki University in 1992 and 1994, respectively. He is currently a Research Associate at Nagasaki University. His main interests have been the analytical method of microstrip antenna and the active antenna.

Kazumasa Tanaka received his B.S., M.S. and Dr.E. degrees in Electronic Communication Engineering, in 1965, 1967, and 1975, respectively, all from Kyushu University, Japan. Since 1981, he has been a professor at Nagasaki University. His main areas of interest include, diffraction of optical beam, detection of optical signal, and optical engineering. Prof. Tanaka is a member of the Japan Society of Applied Physics and Optical Society of America.

Mitsuo Taguchi received his B.E. and M.E. degrees from Saga University in 1975 and 1977, respectively, and a Dr.Eng. degree from Kyushu University in 1986. From 1977 to 1987, he was a Research Associate at Saga University. Since 1987 he has been an Associate Professor at Nagasaki University. In 1996 he was a Visiting Scholar at the Department of Electrical Engineering at the University of California, Los Angeles. His research interests include active antennas, microstrip antennas, and linear antennas. Prof. Taguchi is a member of the IEEE and the Institute of Image Information and Television Engineers.